

Constructive and destructive interaction modes between two tandem flexible flags in viscous flow

SOHAE KIM, WEI-XI HUANG[†]
AND HYUNG JIN SUNG[‡]

Department of Mechanical Engineering, KAIST, 373-1 Guseong-dong,
Yuseong-gu, Daejeon 305-701, Republic of Korea

(Received 16 March 2010; revised 30 June 2010; accepted 30 June 2010;
first published online 2 September 2010)

Two tandem flexible flags in viscous flow were modelled by numerical simulation using an improved version of the immersed boundary method. The flexible flapping flag and the vortices produced by an upstream flag were found to interact via either a constructive or destructive mode. These interaction modes gave rise to significant differences in the drag force acting on the downstream flapping flag in viscous flow. The constructive mode increased the drag force, while the destructive mode decreased the drag force. Drag on the downstream flexible body was investigated as a function of the streamwise and spanwise gap distances, and the bending coefficient of the flexible flags at intermediate Reynolds numbers ($200 \leq Re \leq 400$).

Key words: flow–structure interactions, swimming/flying, wakes

1. Introduction

Avian flocking and fish schooling behaviours have inspired investigations into the fluid dynamics that govern the motion of individuals in the context of a larger group. Fish schooling, which falls within the field of marine propulsion and manoeuvring (Fish 1999; Fish & Lauder 2006), is not merely a social behaviour; schooling improves the efficiency of movement within the fluid environment. Inspired by schooling from a hydrodynamic perspective, a group of aquatic animals can be modelled as a collection of individuals arranged in tandem or side-by-side. In a tandem arrangement, an upstream structure strongly influences a downstream structure through vortex shedding in the fluid medium. The interaction mechanism in a queue has been studied both experimentally and numerically using a variety of rigid body models (Zdravkovich 1985; Streitlien, Triantafyllou & Triantafyllou 1996; Deng, Shao & Yu 2007; Eldredge & Pisani 2008) to show that downstream rigid bodies in a queue gain advantages from the upstream bodies through drag reduction.

Fish and flags, however, are slender flexible bodies that continuously balance the bending forces that act on their bodies via inertia, viscosity and flow pressure. Flexible bodies employ drag reduction mechanisms that differ from those experienced by rigid bodies. Studies using two stationary rigid bodies or flapping rigid bodies within a prescribed range of motion may miss the key beneficial advantages from

[†] Present address: School of Aerospace, Tsinghua University, Beijing 100084, China
[‡] Email address for correspondence: hjsung@kaist.ac.kr

the schooling behaviour of flexible bodies in a fluid flow. Müller (2003) and Zhang *et al.* (2000) recently described the motions of a flexible filament in a flow as a model for fish and flag hydrodynamics. Other studies have described not only a single flag in a flow, but also flags in a side-by-side or tandem arrangement with remarkable results and insights (Zhu & Peskin 2002; Farnell, David & Barton 2004; Connel & Yue 2007; Huang, Shin & Sung 2007; Jia *et al.* 2007; Alben 2008, 2009; Eloy *et al.* 2008; Jia & Yin 2008; Ristroph & Zhang 2008; Michelin & Llewellyn Smith 2009; Schouveiler & Eloy 2009; Zhu 2009). Ristroph & Zhang (2008) showed that in a tandem arrangement of flexible flags, the upstream flag experiences reduced drag relative to the downstream flag. Alben (2009) then displayed this anomalous hydrodynamic drafting in his numerical simulation using an inviscid vortex sheet model. He proposed that the wake behind an upstream flag influences the intensified synchronization of flapping, and the wake-mediated drafting was found to be a function of the gap distance between the flag pairs. Furthermore, Alben (2009) showed that regardless of the gap distance erratic flapping with high-oscillation frequencies does not cause the anomalous drafting in a certain range of the gap distances, which contradicts Ristroph & Zhang (2008). Moreover, Zhu (2009) studied the interaction of two tandem flags in a low-Reynolds-number range ($40 \leq Re \leq 220$). He observed that the upstream flag has less drag than the downstream one (i.e. the anomalous hydrodynamic drafting) when self-sustained flapping is set in, but the opposite when the flags keep the static stretched-straight state at a small enough Reynolds number.

This study provides insights into the manoeuvring dynamics of coupled flexible bodies in viscous flow, with intriguing results: within a queue, the flapping downstream flag can experience a distinct drag reduction and/or a drag enhancement. Moreover, the vortices shed by the upstream flag interact with the downstream flag via two modes of interaction, which explains the significant drag changes experienced by the flexible structures: (i) a constructive mode or (ii) a destructive mode. Although Alben (2009) also reported the constructive and destructive interference between the flags' vortex wakes in inviscid flow, it was obscure how the wakes interact with the downstream flag when the fluid viscosity is included. Obviously, the coupled phenomena become more complicated in viscous flow because vortices could be shed not only from the trailing edge of the flag, but also from the leading edge. The Reynolds numbers selected in this study range from 200 to 400, which are within the gap between the potential flow simulations of Alben (2009) and the small-Reynolds-number simulations of Zhu (2009). The flapping amplitude and the phase difference between two flags were examined with respect to the interaction modes and the drag force. Drag reduction at the downstream flag could be optimized by optimizing the Reynolds number, the streamwise and spanwise gap distances and the bending coefficient of the flexible flags.

2. Computational model

In this paper, a grouping unit consisting of two flexible bodies was modelled using two tandem flexible flags in a two-dimensional viscous flow. A schematic diagram of the configuration and coordinate system is shown in figure 1. The relative positioning of the two tandem flexible flags was varied by adjusting the streamwise gap distance G_x and the spanwise gap distance G_y , defined relative to the initial tail position of the upstream flag. The heads of both upstream and downstream flags were fixed under a simply supported boundary condition; boundary conditions for a free end were considered at the tails. An Eulerian coordinate system was

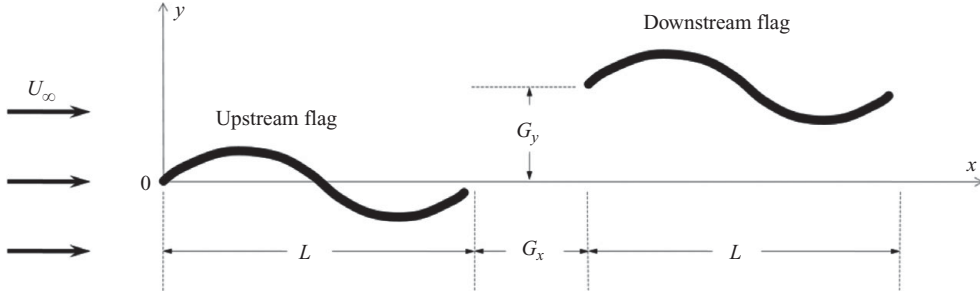


FIGURE 1. Schematic diagram of the two tandem flags in viscous flow.

used to describe the uniform flow, and a separate Lagrangian coordinate system was applied to each flexible flag. The tandem flexible flags in viscous flow were modelled using an improved version of the immersed boundary method (Huang *et al.* 2007). The immersed boundary method solved the equations governing fluid flow and the two flexible flag motions in each coordinate system, and the interactions among components were calculated using a feedback force law. Huang *et al.* (2007) simulated a single flexible filament and two filaments in a side-by-side arrangement in a uniform flow, assuming inextensibility in the filaments. Because the same method was used here, with the only difference being the mutual arrangement of the filaments, the validity of the model will be assumed in the following discussion.

The incompressible viscous fluid flow was described using the Navier–Stokes and continuity equations, which were non-dimensionalized by the far-field velocity U_∞ to yield the velocity vector $\mathbf{u} = (u, v)$ as a function of time $t = L/U_\infty$ (where L is the length of the flag), pressure $p = \rho_0 U_\infty^2$ (where ρ_0 is the fluid volume density) and the momentum force $\mathbf{f} = (f_x, f_y)/(\rho_0 U_\infty^2/L)$:

$$\frac{\partial \mathbf{u}}{\partial t} + \mathbf{u} \cdot \nabla \mathbf{u} = -\nabla p + \frac{1}{Re} \nabla^2 \mathbf{u} + \mathbf{f}, \quad (2.1)$$

$$\nabla \cdot \mathbf{u} = 0, \quad (2.2)$$

where the Reynolds number Re is defined by $Re = \rho_0 U_\infty L / \mu$ and μ is the dynamic viscosity. Equations (2.1) and (2.2) were solved by using the fractional-step method with a staggered Cartesian grid system (Kim, Baek & Sung 2002). Similar to the equations of Huang *et al.* (2007), the governing equations for the inextensible flexible flag were non-dimensionalized by the following characteristic scales: the flag length L defined the unit of length, L/U_∞ defined the unit of time, $\rho_1 U_\infty^2/L$ defined the units of Lagrangian force \mathbf{F} (where the flag line density is $\rho_1 + \rho_0 A$ with A the thickness of flag), $\rho_1 U_\infty^2$ defined the tension force T and $\rho_1 U_\infty^2 L^2$ defined the bending rigidity γ . The flag motion was, therefore, described by

$$\frac{\partial^2 \mathbf{X}}{\partial t^2} = \frac{\partial}{\partial s} \left(T \frac{\partial \mathbf{X}}{\partial s} \right) - \frac{\partial^2}{\partial s^2} \left(\gamma \frac{\partial^2 \mathbf{X}}{\partial s^2} \right) - \mathbf{F}, \quad (2.3)$$

where s is the arclength and $\mathbf{X} = (X(s, t), Y(s, t))$ is the position. At the fixed and free ends, the following boundary conditions were applied:

$$\mathbf{X} = \mathbf{X}_0, \quad \frac{\partial^2 \mathbf{X}}{\partial s^2} = (0, 0) \quad \text{for the fixed end}, \quad (2.4)$$

$$T = 0, \quad \frac{\partial^2 \mathbf{X}}{\partial s^2} = (0, 0), \quad \frac{\partial^3 \mathbf{X}}{\partial s^3} = (0, 0) \quad \text{for the free end}. \quad (2.5)$$

The interaction force between the flow and the structure was calculated using the feedback force

$$\mathbf{F} = \alpha \int_0^t (\mathbf{U}_{ib} - \mathbf{U}) d\tau + \beta(\mathbf{U}_{ib} - \mathbf{U}), \quad (2.6)$$

where α and β are large negative free constants -10^5 and -10^3 , respectively, in Huang *et al.* (2007). \mathbf{U}_{ib} is the fluid velocity obtained by interpolation at the immersed boundary and \mathbf{U} is the velocity of the flag expressed by $\mathbf{U} = d\mathbf{X}/dt$. The following interpolation relations between the Eulerian and Lagrangian values are carried out by the same Dirac delta function as in Huang *et al.* (2007):

$$\mathbf{U}_{ib}(s, t) = \int_{\Omega} \mathbf{u}(\mathbf{x}, t) \delta(\mathbf{X}(s, t) - \mathbf{x}) d\mathbf{x}, \quad (2.7)$$

$$\mathbf{f}(\mathbf{x}, t) = \frac{\rho_1}{\rho_0 L} \int_{\Gamma} \mathbf{F}(s, t) \delta(\mathbf{x} - \mathbf{X}(s, t)) ds. \quad (2.8)$$

Note that use of the Dirac delta function smears the fluid–structure interface, which makes the method unsuitable for high-Reynolds-number flow. However, it has no difficulty in simulating fluid–structure interactions at Reynolds number of several hundred, as reported in a series of previous studies (Peskin 2002; Huang *et al.* 2007; Shin, Huang & Sung 2008). It should also be noted that selection of large negative values of α and β in calculating the feedback force (see (2.6)) may result in a stiff problem (Goldstein, Handler & Sirovich 1993). However, in our improved version of the immersed boundary method, it was shown that the limitation on the computational time step can be significantly relieved by selecting the Lagrangian points for velocity interpolation and the smoothed delta function appropriately (Huang *et al.* 2007; Shin *et al.* 2008).

The computational domain for the fluid flow ranges from -2 to 6 in the streamwise (x) direction and -4 to 4 in the spanwise (y) direction, which are characterized by the flag length. The Eulerian grid size for the fluid is 512×250 and the Lagrangian grid size for the flag is 64 . The Eulerian grid is uniformly distributed in the x direction, while in the y direction it is uniform for $-1 \leq y \leq 1$ but is stretched otherwise. The initial position of the upstream flag is parallel to the streamwise direction and the downstream one is inclined as much as 0.1π from the streamwise direction. Even if the inclination is changed to -0.1π , the results after several transient periods are not changed. The computational time step is set to be 0.0005 in all the simulations, which results in a Courant number of about 0.1 . The flow patterns were investigated by conducting simulations over a long time period, between 100 and 500 flapping periods, and the flow patterns obtained after a minimum of 20 equilibration flapping periods were analysed. The flow patterns and interaction forces were characterized by averaging the drag coefficient C_d , the flapping amplitude A_{tail} and the phase difference between the two flapping flags $\Delta\phi$ (figures 2, 5 and 6). The quantitative characterizations of the interaction behaviour were supplemented by qualitative evaluations of the flag deformations (figure 3), the vorticity contours and the pressure fields within the flow (figure 4), which provide an intuitive understanding of the vortex–flexible-body interaction. Four parameters were chosen for optimization within the following ranges: the Reynolds number ($200 \leq Re \leq 400$), the streamwise ($0.1 \leq G_x \leq 2.0$) and spanwise ($-0.45 \leq G_y \leq 0.45$) gap distances between the flags and the bending coefficient of the flags ($0.001 \leq \gamma \leq 0.008$).

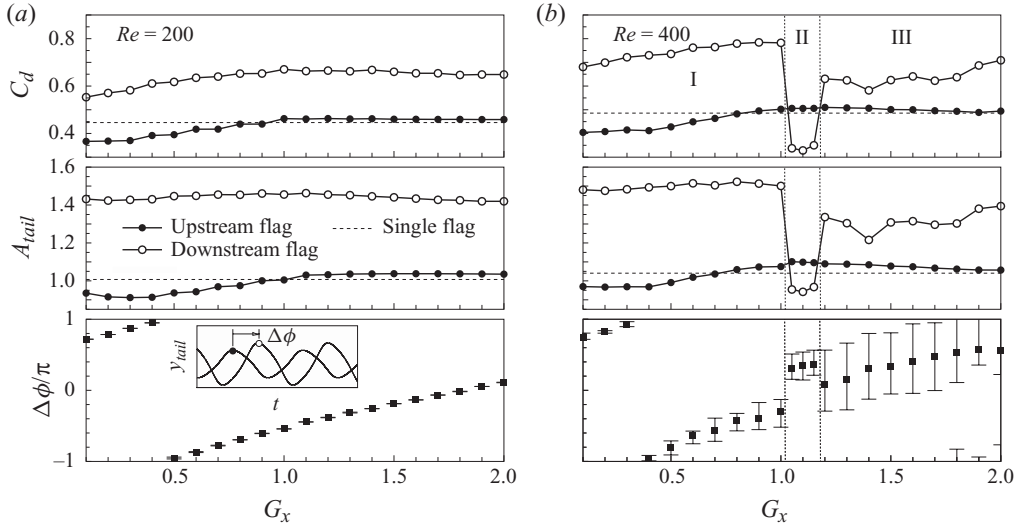


FIGURE 2. Drag coefficient (C_d), the flapping amplitude of the tail (A_{tail}) and the phase difference between the flapping of the two flags ($\Delta\phi$) as a function of the streamwise gap distance (G_x) for $\gamma = 0.005$ and $G_y = 0.0$. In plots for the phase difference, black squares indicate the average values of the phase difference and the error bars indicate the minimum and maximum values: (a) $Re = 200$ and (b) $Re = 400$.

3. Results and discussion

The drag coefficient C_d , the flapping amplitude of the tails A_{tail} and the phase difference between flags $\Delta\phi$ are plotted in figure 2 as a function of the streamwise gap distance G_x . The plots demonstrate two salient features of the system. The first salient feature is that the downstream flag experiences drag reduction within a specific range of the streamwise gap distance, although Ristroph & Zhang (2008) reported that the flexible flags show the anomalous hydrodynamic drafting in which the upstream body experiences drag reduction, but the downstream body does not. For the parameter range $1.05 \leq G_x \leq 1.15$ and $Re = 400$ (regime II) in figure 2(b), the drag coefficient of the downstream flag dropped sharply below that of the upstream flag. Under such conditions, the drag coefficient of the downstream flag decreased to as much as 65% of the upstream drag coefficient. Anomalous hydrodynamic drafting was observed for $Re = 200$ across the full range of tested streamwise gap distances. Although anomalous hydrodynamic drafting was also observed across a range of small streamwise gap distances ($G_x \leq 1.0$) for $Re = 400$ (regime I in figure 2b), we propose that drag reduction within regime II in figure 2(b) arose from an interaction mode that was distinct from that operating at $Re = 200$. The second salient feature of the system is that anomalous hydrodynamic drafting was observed for $G_x \geq 1.2$, $Re = 400$ (regime III) in figure 2(b). In regime III, the drag increase on the downstream flag was only 25%, not as significant as the drag increase observed in the regime I (75% increase of the drag on the downstream flag). The mechanism underlying the reduction in the downstream drag coefficient will be discussed below in figure 4, considered together with the phase difference between two flags in figures 2 and 5.

As shown in figure 2, the dependence of the drag coefficient on G_x was similar to the dependence of the flapping amplitude on G_x , which implied that the drag forces on the flags were related to the flapping amplitudes: the more widely the flags flapped,

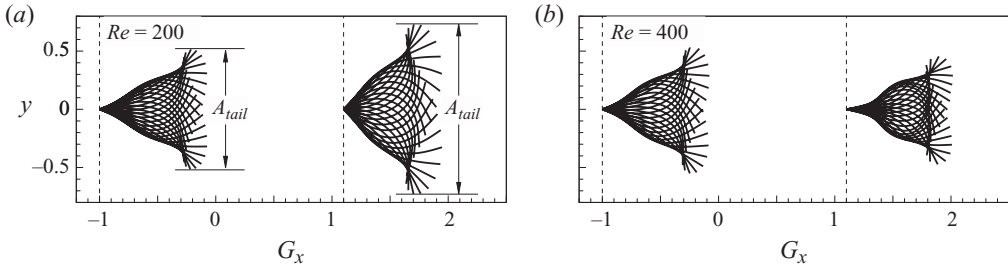


FIGURE 3. Traces of the two tandem flags over one period of flapping for $\gamma = 0.005$, $G_x = 1.1$ and $G_y = 0.0$: (a) $Re = 200$ and (b) $Re = 400$.

the more drag force they experienced. The relationship between the drag coefficient and the flapping amplitude was inferred from the shape of the flag deformation, as shown in figure 3. Each Reynolds number yielded distinct deformation geometries in the downstream flag, although the shapes of the upstream flag were similar. For $Re = 200$, the downstream flag flapped with larger amplitude than the upstream flag did, in agreement with the results of Ristroph & Zhang (2008). Because the wake behind the first flag drove synchronization in the flapping of the downstream flag (Alben 2009), the large flapping amplitude caused the downstream flag to experience more drag force than the upstream flag. By contrast, at $Re = 400$, the downstream flag flapped with a smaller amplitude than the upstream flag, and the head of the downstream flag encountered a wake with an angle of attack that approached zero. Therefore, the drag force acting on the downstream flag was reduced relative to the drag force acting on the upstream flag. It is interesting that the downstream flag deformations showed different degrees of concavity and convexity at $Re = 200$ and at $Re = 400$, because the bending coefficients were identical in the two cases. The different degrees of flag deformations at a constant bending coefficient resulted solely from variations in the Reynolds number.

Variations in the relative deformations and drag forces in the upstream and downstream flags can be explained, from a hydrodynamic perspective, as arising from two interaction modes, as illustrated in figure 4. The interaction between tandem flags and a flow influences the forces experienced by the flags via one of the two modes: (i) a constructive mode and (ii) a destructive mode. These interaction modes were first described by Gopalkrishnan *et al.* (1994) as part of their investigation of active vorticity control using a flapping foil behind a circular cylinder in a flow. In that study, the authors identified three modes of interaction and noted that the cylinder vortices were repositioned by the suction produced by the foil. In this paper, the constructive mode describes the situation in which vortices that surround and are shed by the downstream structure merge with vortices of the same rotational sense produced by the upstream structure. The act of merging produces vortices of higher strength. In contrast, the destructive mode describes merging of vortices of the opposite sense, produced by the upstream and downstream structures. The strength of the merged vortex is decreased.

As shown in figure 4(c, d), the positions that experienced the maximum or zero transverse displacements of the downstream tail, y_{tail} , are marked, respectively, as A and B within one period of flapping, and these points correspond, respectively, to the maximum and minimum drag coefficients. Instantaneous vorticity contours at positions A and B are presented in figure 4(a, b) for both the constructive and

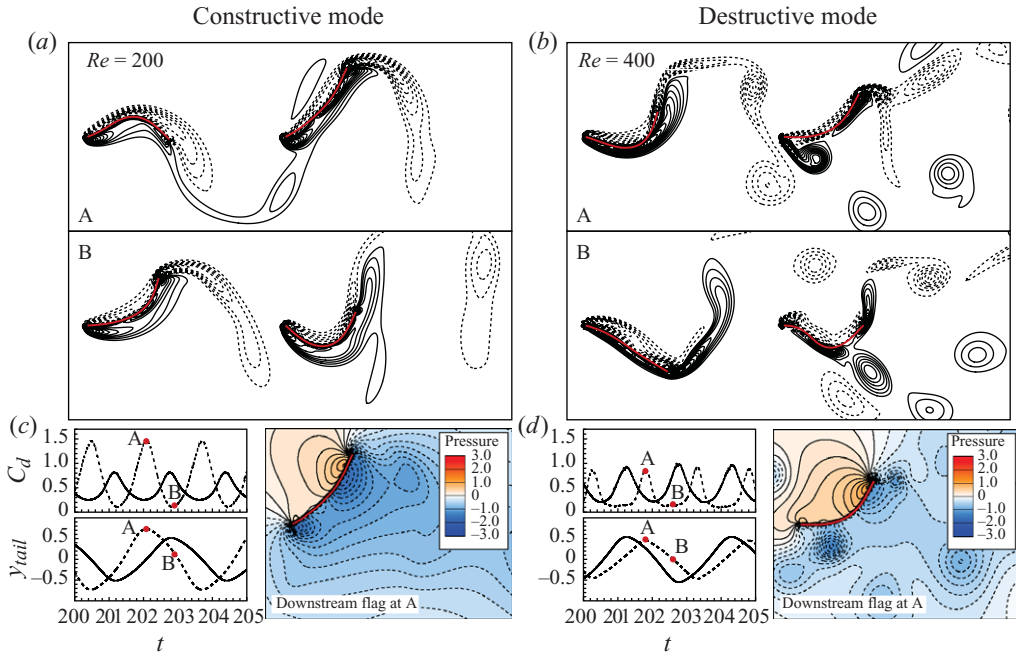


FIGURE 4. (Colour online) Two sets of figures are presented in the left and right columns for the constructive and destructive modes, respectively, for $\gamma = 0.005$, $G_x = 1.1$ and $G_y = 0.0$: (a, c) $Re = 200$ and (b, d) $Re = 400$. The column for each mode contains three plots: (a, b) the instantaneous vorticity contours at the positions A and B; (c, d) the time history of the drag coefficient and the transverse displacement of the upstream tail (solid line) and downstream tail (dashed line), and the pressure field of the flow surrounding the downstream flag at the position A.

destructive modes. Under the constructive mode, the downstream flag encountered incoming counter-clockwise vortices, while the flaps were driven by the incoming vortices. The downstream flapping was not only driven by the vortices produced by the downstream flag, but also by the incoming vortices, which merged constructively to increase the amplitude of flapping. Under the destructive mode, however, counter-clockwise vortices that had been shed from the head of the downstream flag encountered incoming clockwise vortices, while the flaps were driven by the incoming vortices. The vortices merged destructively and were subsequently weakened, decreasing the amplitude of the downstream flag-flapping motion. The drag force was directly investigated by calculating the pressure field in the flow surrounding the downstream flag, as shown in figure 4(c, d). Constructively merged vortices intensified the restoring force for the flapping of the downstream flag, whereas destructively merged vortices weakened the restoring force for the flapping motion.

The transition between the two modes was governed by the phase difference that characterized the periodic motion of the two flags, as shown in figure 2. For simplicity, the phase difference was defined as a function of the relative transverse displacements of the flag tails. The phase difference between the motion of the flags dictated the phase in which the downstream flag encountered the vortices. For $Re = 200$, the phase difference depended linearly on the streamwise gap distance and was almost unchanged. By contrast, $Re = 400$ yielded behaviour within the specific streamwise gap range of regime II ($1.05 \leq G_x \leq 1.15$ for $Re = 400$) that differed significantly from the behaviour observed at $Re = 200$ in terms of the averaged phase difference,

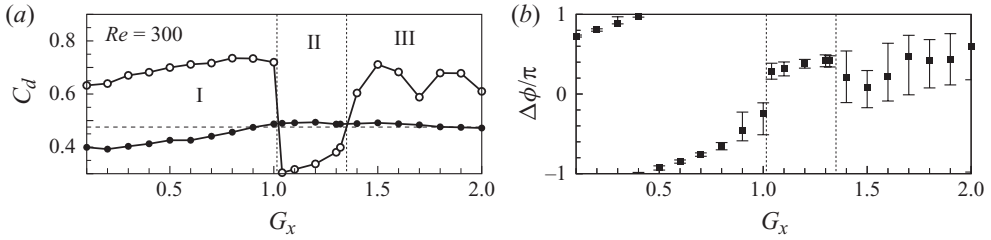


FIGURE 5. Drag coefficient and the phase difference as a function of the streamwise gap distance for $Re = 300$, $\gamma = 0.005$ and $G_y = 0.0$. Refer to figure 2 for the meaning of symbols.

although in regime I the behaviour resembled that observed for $Re = 200$. Moreover, in regime III ($G_x \geq 1.2$, $Re = 400$) the phase difference varied from a value similar to that observed at $Re = 200$ to the value plus a factor of π . The instantaneous vorticity contours demonstrated that the constructive mode was in operation when the phase difference was similar to that observed for $Re = 200$ and the destructive mode was in operation otherwise. In other words, tandem flags experienced alternating constructive and destructive modes in regime III ($G_x \geq 1.2$ and $Re = 400$) and the alternating frequency of the modes is inferred from the maximum, minimum and averaged value of the phase difference in figure 2. Moreover, the destructive mode produced a stable state for cases in which the averaged value jumped, for example, in regime II ($1.05 \leq G_x \leq 1.15$ for $Re = 400$). Depending on whether the system was characterized by either the stable constructive or destructive modes or whether the system alternated between modes, the averaged drag coefficient experienced by the downstream flag increased, decreased or increased by a factor of $1/2$, as shown in figure 2.

Figures 2 and 4 show that the vortex shed from the head of the downstream flag destabilized the flapping motion and phase shifted the flapping motion for $Re = 400$. As a consequence, the vortex shed from the head of the flag initiated the transition between constructive and destructive modes. For a potential flow, Alben (2009) showed that the averaged phase difference decreases with a nearly constant slope as the streamwise gap distance increases, and showed some variation with irregular flapping of the downstream flag near regimes II and III of this study. Viscosity, however, smoothes out vortices that are encountered by the downstream flag and damps out the irregular flapping motion. The downstream flag in a viscous flow shows a regular flapping under the destructive mode as well as under the constructive mode in this study. The effect of viscosity is further inspected in figure 5. For $Re = 300$, the difference between maximum and minimum values of the phase difference is reduced in regime III compared with that of $Re = 400$ in figure 2. In addition, the streamwise gap distance range for regime II is extended to $1.05 \leq G_x \leq 1.32$, while regime II is within $1.05 \leq G_x \leq 1.15$ for $Re = 400$. This means that viscosity plays an important role to make the flapping set in at one of the two modes. Regardless of the initial inclination of flags, the phase difference varies from the values for the constructive mode to the values plus a factor of π in regimes II and III for the destructive mode. After several transient flapping periods, the phase is fixed to the destructive mode only in regime II, while the phase varies between the values for each mode alternately in regime III; keeping to one mode in regime II and alternation between two modes in regime III are strongly influenced by viscosity.

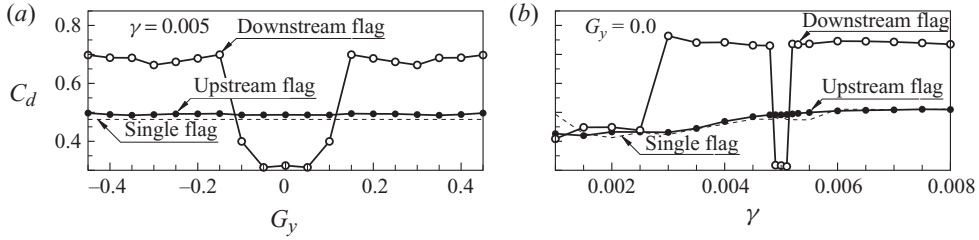


FIGURE 6. Drag coefficient variation as a function of the spanwise gap distance, G_y , and the bending coefficient, γ , for $Re = 300$ and $G_x = 1.1$: (a) $\gamma = 0.005$ and (b) $G_y = 0.0$.

The spanwise gap distance, G_y , and the bending coefficient, γ , dictated whether the downstream flag experienced either the constructive or the destructive mode, as indicated by the drag coefficient shown in figure 6, calculated for $Re = 300$ and $G_x = 1.1$. For $\gamma = 0.005$, the flag experienced a drag reduction in the range $|G_y| \leq 0.1$. The bending coefficient γ of the flags described in this study is related to the ratio between the flag rigidity, R_2 and the dimensionless mass of the flag, R_1 described in Alben (2009) by the following relation:

$$\gamma = \frac{R_2}{4R_1}. \quad (3.1)$$

Alben (2009) assumed that $R_1 = 0.6$ and $R_2 = 0.014$, which corresponds to $\gamma = 0.00583$ in this paper, and showed some variations as a function of the gap distance. For $R_1 = 0.6$ and $R_2 = 0.011$ ($\gamma = 0.00458$ in this paper), the downstream flag irregularly flaps with small flapping amplitude and short flapping period regardless of the gap distance. As shown in Alben (2009), flexible flags cannot sustain regular flapping motions when forces on the flexible body are put into imbalance as a result of fluid pressure, viscosity, the flag inertia and the bending coefficient. Therefore, if a flexible body with an optimal bending coefficient is positioned behind a flexible body in a flow with an appropriate gap distance, the trailing body can obtain a significant advantage with respect to drag reduction. For example, fish might have evolved to optimize their self-adaptive bending coefficients in order to maximize the efficiency of the vortex–flexible-body interaction modes. Because the present calculation is based on two-dimensional flow and is restricted to large-Reynolds-number simulations, quantitative predictions of the parameters that optimize fish manoeuvring cannot be obtained. This study, however, qualitatively characterized the relationship between the drag force and the two modes of vortex–flexible-body interaction: (i) the drag was increased on the downstream body under the constructive mode and (ii) the drag was reduced on the downstream body under the destructive mode.

4. Conclusions

Two tandem flexible flags in viscous flow were modelled by numerical simulation using an improved version of the immersed boundary method. The downstream flag experienced a range of conditions as a function of the streamwise and spanwise gap distances, and the bending coefficient for $200 \leq Re \leq 400$. In addition to the drag increase predicted by previous studies, the drag on the downstream flexible body was found to decrease within a specific range of parameters. The drag on the downstream body was found to result from the interaction between the vortices and the flexible flag. The position at which vortices were shed by a downstream flag was affected

by the flag flexibility and the deformation. Vortices shed at the head of a flag destabilized the flapping motion by interacting with the wake of the upstream flag. Therefore, the phase with which the downstream flag encountered vortices varied, and different modes of interaction (constructive and destructive modes) between vortices and a flexible flag were observed. In this study, the two interaction modes produced opposite effects on the drag force experienced by the downstream flag: (i) the constructive mode increased the drag and (ii) the destructive mode decreased the drag. The relationship between the drag force and the interaction modes of the vortex–flexible-body system suggests a mechanism for the advantages gained by the hydrodynamic manoeuvring in schools of flexible bodies.

This work was supported by the Creative Research Initiatives (Center for Opto–Fluid–Flexible Body Interaction) and the World Class University (WCU) program of MEST/NRF.

REFERENCES

- ALBEN, S. 2008 Flapping states of a flag in an inviscid fluid: bistability and the transition to chaos. *Phys. Rev. Lett.* **100**, 074301.
- ALBEN, S. 2009 Wake-mediated synchronization and drafting in coupled flags. *J. Fluid Mech.* **641**, 489–496.
- CONNELL, B. S. H. & YUE, D. K. P. 2007 Flapping dynamics of a flag in a uniform stream. *J. Fluid Mech.* **581**, 33–67.
- DENG, J., SHAO, X.-M. & YU, Z.-X. 2007 Hydrodynamic studies on two traveling wavy foils in tandem arrangement. *Phys. Fluids* **19**, 113104.
- ELDRIDGE, J. D. & PISANI, D. 2008 Passive locomotion of a simple articulated fish-like system in the wake of an obstacle. *J. Fluid Mech.* **611**, 97–106.
- ELOY, C., LAGRANGE, R., SOUILLIEZ, C. & SCHOUVEILER, L. 2008 Aeroelastic instability of cantilevered flexible plates in uniform flow. *J. Fluid Mech.* **611**, 97–106.
- FARNELL, D. J. J., DAVID, T. & BARTON, D. C. 2004 Coupled states of flapping flags. *J. Fluid. Struct.* **19**, 29–36.
- FISH, F. E. 1999 Energetics of swimming and flying in formation. *Comments Theor. Biol.* **5**, 283–304.
- FISH, F. E. & LAUDER, G. V. 2006 Passive and active flow control by swimming fishes and mammals. *Annu. Rev. Fluid Mech.* **38**, 193–224.
- GOLDSTEIN, D., HANDLER, R. & SIROVICH, L. 1993 Modeling a no-slip flow boundary with an external force field. *J. Comput. Phys.* **105**, 354–366.
- GOPALKRISHNAN, R., TRIANTAFYLLOU, M. S., TRIANTAFYLLOU, G. S. & BARRETT, D. 1994 Active vorticity control in a shear flow using a flapping foil. *J. Fluid Mech.* **274**, 1–21.
- HUANG, W.-X., SHIN, S. J. & SUNG, H. J. 2007 Simulation of flexible filaments in a uniform flow by the immersed boundary method. *J. Comput. Phys.* **226**, 2206–2228.
- JIA, L.-B., LI, F., YIN, X.-Z. & YIN, X.-Y. 2007 Coupling modes between two flapping filaments. *J. Fluid Mech.* **581**, 199–220.
- JIA, L.-B. & YIN, X.-Z. 2008 Passive oscillations of two tandem flexible filaments in a flowing soap film. *Phys. Rev. Lett.* **100**, 228104.
- KIM, K., BAEK, S.-J. & SUNG, H. J. 2002 An implicit velocity decoupling procedure for the incompressible Navier-Stokes equations. *Intl J. Numer. Meth. Fluids* **38**, 125–138.
- MICHELIN, S. & LLEWELLYN SMITH, S. G. 2009 Linear stability analysis of coupled parallel flexible plates in an axial flow. *J. Fluid. Struct.* **25**, 1136–1157.
- MÜLLER, U. K. 2003 Fish'n flag. *Science* **302**, 1511–1512.
- PESKIN, C. S. 2002 The immersed boundary method. *Acta Numerica* **11**, 479–517.
- RISTROPH, L. & ZHANG, J. 2008 Anomalous hydrodynamic drafting of interacting flapping flags. *Phys. Rev. Lett.* **101**, 194502.
- SCHOUVEILER, L. & ELOY, C. 2009 Coupled flutter of parallel plates. *Phys. Fluids* **21**, 081703.

- SHIN, S. J., HUANG, W.-X. & SUNG, H. J. 2008 Assessment of regularized delta functions and feedback forcing schemes for an immersed boundary method. *Intl J. Numer. Methods Fluids* **58**, 263–286.
- STREITLIEN, K., TRIANTAFYLLOU, G. S. & TRIANTAFYLLOU, M. S. 1996 Efficient foil propulsion through vortex control. *AIAA J.* **34**, 2315–2319.
- ZDRAVKOVICH, M. M. 1985 Flow induced oscillations of two interfering circular cylinders. *J. Sound Vib.* **101**, 511–521.
- ZHANG, J., CHILDRESS, S., LIBCHABER, A. & SHELLEY, M. 2000 Flexible filaments in a flowing soap film as a model for one-dimensional flags in a two-dimensional wind. *Nature* **408**, 835–839.
- ZHU, L. 2009 Interaction of two tandem deformable bodies in a viscous incompressible flow. *J. Fluid Mech.* **635**, 455–475.
- ZHU, L. & PESKIN, C. S. 2002 Simulation of a flapping flexible filament in a flowing soap film by the immersed boundary method. *J. Comput. Phys.* **179**, 452–468.